ARMY RESEARCH LABORATORY

Control Mechanism Strategies for Spin-Stabilized Projectiles

by Frank Fresconi and Peter Plostins

NOTICES

Disclaimers

The findings in this report are not to be construed as an official Department of the Army position unless so designated by other authorized documents.

Citation of manufacturer's or trade names does not constitute an official endorsement or approval of the use thereof.

Destroy this report when it is no longer needed. Do not return it to the originator.

Army Research Laboratory

Aberdeen Proving Ground, MD 21005-5066

Control Mechanism Strategies for Spin-Stabilized Projectiles

Frank Fresconi and Peter Plostins
Weapons and Materials Research Directorate, ARL

REPORT DOCUMENTATION PAGE		Form Approved OMB No. 0704-0188

Public reporting burden for this collection of information is estimated to average 1 hour per response, including the time for reviewing instructions, searching existing data sources, gathering and maintaining the data needed, and completing and reviewing the collection information. Send comments regarding this burden estimate or any other aspect of this collection of information, including suggestions for reducing the burden, to Department of Defense, Washington Headquarters Services, Directorate for Information Operations and Reports (0704-0188), 1215 Jefferson Davis Highway, Suite 1204, Arlington, VA 22202-4302. Respondents should be aware that notwithstanding any other provision of law, no person shall be subject to any penalty for failing to comply with a collection of information if it does not display a currently valid OMB control number.
PLEASE DO NOT RETURN YOUR FORM TO THE ABOVE ADDRESS.

1. REPORT DATE (DD-MM-YYYY)	2. REPORT TYPE	3. DATES COVERED (From - To)
September 2008	Final	January 2008–May 2008

4. TITLE AND SUBTITLE	5a. CONTRACT NUMBER
Control Mechanism Strategies for Spin-Stabilized Projectiles	
	5b. GRANT NUMBER
	5c. PROGRAM ELEMENT NUMBER
6. AUTHOR(S)	5d. PROJECT NUMBER
Frank Fresconi and Peter Plostins	AH43
	5e. TASK NUMBER
	5f. WORK UNIT NUMBER

7. PERFORMING ORGANIZATION NAME(S) AND ADDRESS(ES)	8. PERFORMING ORGANIZATION REPORT NUMBER
U.S. Army Research Laboratory ATTN: AMSRD-ARL-WM-BC Aberdeen Proving Ground, MD 21005-5066	ARL-TR-4611

9. SPONSORING/MONITORING AGENCY NAME(S) AND ADDRESS(ES)	10. SPONSOR/MONITOR'S ACRONYM(S)
	11. SPONSOR/MONITOR'S REPORT NUMBER(S)

12. DISTRIBUTION/AVAILABILITY STATEMENT

Approved for public release; distribution is unlimited.

13. SUPPLEMENTARY NOTES

14. ABSTRACT

Spin-stabilized artillery munitions were originally designed to provide precise ballistic fire on long-range targets. Today the challenge is to utilize these ballistic munitions in military operations in urban terrain environments where significantly higher levels of precision are required to minimize collateral damage. One strategy is to retrofit these munitions with some level of low-cost precision. Unique challenges arise when munitions designed to be ballistically precise are guided. Projectile flight is often stabilized by a high spin rate, which induces complex dynamics. Flight mechanics are further aggravated by adding a control mechanism. The goal of this study was to provide a fundamental understanding of various control mechanism strategies for spin-stabilized projectiles. Flight control systems were developed and executed in a six degree-of-freedom simulation. Formulating a generalized model of a control mechanism allowed investigation of parameters such as control force magnitude, control axial location, control lift-to-drag ratio, and control force duration. Results showed that control authority linearly related to control force magnitude. Maximal control authority was obtained by placing the control mechanism at the rear of the projectile. The variation with axial location was also determined since these results were valuable for instances when the control was unable to be located near the projectile base. A lower lift-to-drag ratio of the control mechanism decreased control authority and maximum range. Lastly, the trade-offs associated with continuous and pulsed flight control systems were quantified. Physical explanations for the simulation results were provided.

15. SUBJECT TERMS

flight dynamics, precise munition, aerodynamics, spin-stabilized projectile

16. SECURITY CLASSIFICATION OF:			17. LIMITATION OF ABSTRACT	18. NUMBER OF PAGES	19a. NAME OF RESPONSIBLE PERSON Frank Fresconi
a. REPORT	b. ABSTRACT	c. THIS PAGE	SAR	34	19b. TELEPHONE NUMBER (Include area code) 410-306-0794
UNCLASSIFIED	UNCLASSIFIED	UNCLASSIFIED			

Standard Form 298 (Rev. 8/98)
Prescribed by ANSI Std. Z39.18

Contents

List of Figures

List of Tables

INTENTIONALLY LEFT BLANK.

1. Introduction

Many current low-intensity conflicts occur in military operations in urban terrain (MOUT) environments and require precise fires against small and fleeting targets. Low collateral damage is now a mission requirement since the opposition forces are generally intermingled with the local civilian population. Using precision munitions, laser-guided bombs, and/or guided missiles is very effective but represents a very high-cost option.

An alternate strategy is to retrofit current stockpiles of low-cost ballistic munitions using their intrinsic ballistic accuracy to enable a cost-effective precision engagement solution. However, there are some basic physics and engineering challenges that need to be addressed and understood if choosing this path. The luxury of designing guided munitions from scratch is that the maneuverability can be designed and optimized into the system. However, retrofitting a munition with a guidance package that was originally designed for a ballistic mission and is inherently ultrastable constrains the maneuver capability. This constraint is controlled by the fundamental flight dynamics of the original munition design. This report looks at some of the fundamental physics of this problem as it relates to retrofitting spin-stabilized artillery munitions with various guidance package options.

Requirements for the retrofit of spin-stabilized munitions exist in the gun-launched community. This environment is sufficiently different from more traditional smart weapons, thus warranting basic research into guidance and control strategies. Conventional methods include canards, fins, and wings. Furthermore, in many conventional applications, the projectile is fin stabilized (i.e., the center of pressure of aerodynamic force is aft of the center of gravity [CG]) and the roll rate is either low or held zero by an active flight control system. For spin-stabilized, gun-launched munitions, the projectile is statically unstable (i.e., the center of pressure of aerodynamic force is forward of the CG) and must be stabilized by gyroscopic action. High spin rates typically result. The flight dynamics of these munitions often involve complex phenomena such as nonlinear Magnus moments and yaw of repose. Adding a control mechanism such as fins to guide a spin-stabilized projectile further complicates the resulting motion. Actuation of the control mechanism at high spin rates is another potential obstacle to developing spin-stabilized precision munitions.

Ollerenshaw and Costello[1] obtained expressions for the swerve response of projectiles with control input that showed the optimal location of the control force for a fin- and spin-stabilized projectile. This effort also demonstrated that the phase shift of the swerve response for a spin-stabilized projectile is close to 0° or 180°, depending on the location of the control mechanism.

---

[1]Ollerenshaw, D.; Costello, M. *On the Swerve Response of Projectiles to Control Input*; ARL-CR-0604; U.S. Army Research Laboratory: Aberdeen Proving Ground, MD, April 2008.

Frost and Costello[2] investigated the control authority of a projectile equipped with an internal unbalanced part. Corriveau et al.[3] studied the drift magnitude and direction on an artillery round due to one or more thrusters with various levels of impulse.

The objective of this effort is to elucidate the role of various control mechanism parameters on the performance of spin-stabilized projectiles. This allows optimization of the control mechanism and a practical understanding of the trade-offs involved with a suboptimal control mechanism designed to accommodate another munition subsystem such as a warhead or rocket motor.

To accomplish this goal, a spin-stabilized, indirect-fire munition was selected for this study. The results were typical for this class of projectile. Rather than choose particular control mechanisms, a general model was developed to illustrate universal trends. Two flight control systems were designed—a continuous system with an inertially fixed control mechanism which applied control forces and moments throughout the entire roll cycle (to model a despun control mechanism) and a pulsed system featuring a body-fixed control mechanism which operated only during portions of the roll cycle.

These controllers were implemented in a six degree-of-freedom simulation to assess the impact of various control strategies on the flight dynamics and overall performance. Specific control mechanism parameters investigated included the magnitude of the control normal force, the control axial location on the projectile, the control normal-to-axial force ratio (or lift-to-drag ratio), and the roll window over which the pulsed controller operated. The metrics of this analysis were the maneuver footprint, total angle of attack (AOA), and range.

For this study, a control mechanism is defined as the effector inducing a maneuver in the flight vehicle. As discussed, common control mechanism are canards, fins, and wings. Examples of less conventional control mechanisms may include thrusters, ducted air flows, and moveable surfaces such as tabs and noses. Electromagnetic devices such as stepper motors, solenoids, and voice coils are often used to actuate these control mechanisms.

The control mechanism modeling, flight control system development, and analysis approach are described in the next section. The results of this effort are then presented, followed by a summary of the influence of each control mechanism parameter on control authority.

---

[2]Frost, G.; Costello, M. Control Authority of a Projectile Equipped with an Internal Unbalanced Part. *Journal of Dynamic Systems, Measurement, and Control* **2006**, *128*, 1005–1012.

[3]Corriveau, D.; Berner, C.; Fleck, V. Trajectory Correction Using Impulse Thrusters for Conventional Artillery Projectiles, *23rd International Symposium on Ballistics*, Tarragona, Spain, April 2007.

2. Modeling and Methodology

The projectile physicals used for this analysis are given in table 1. The aerodynamics package for this projectile consists of coefficients for axial force, normal force, Magnus force, pitching moment, pitch damping moment, roll damping moment, and Magnus moment. These physicals and aerodynamics are typical of a 155-mm artillery round.

Table 1. Physical parameters.

Weight (kg)	Axial Inertia (kg-m²)	Transverse Inertia (kg-m²)	Center of Gravity From Nose (mm)	Diameter (mm)	Overall Length (mm)
46.17	0.1706	2.034	552.7	154.7	843.3

A general model of a control mechanism was formulated since any control event results in a force and a moment at some location on the projectile. For example, the deflection of a canard near the nose of a projectile produces forces normal and axial to the control surface. The distance between the CG and the location of these forces on the canard is a moment arm by which the resulting forces are multiplied to obtain a moment on the projectile. This type of argument can be extended to any control mechanism.

The general model is illustrated in figure 1. In this figure, N_C is the control normal force, A_C is the control axial force, X_C is the axial location of the control, and M_C is the resulting control moment. Positive X_C is forward of the CG, and the point of application of the control forces is assumed on the spin axis of the projectile.
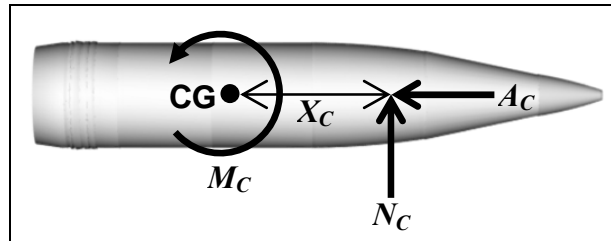

Figure 1. General model of a control mechanism.

In reality, the control forces and moments may be due to an aerodynamic effect such as the deflection of a fin. However, for this study, they are referred to as control forces and moments. The aerodynamics of the entire projectile configuration are treated separately from the control mechanism. This leads to a critical assumption in the control mechanism model. A control mechanism which affects the flow around the projectile (e.g., canards and fins) would shift the

location of the center of pressure (CP). In this study, the CP location is not adjusted due to control forces. The consequence of this assumption is that the dynamics will be somewhat different in this situation due to different moments produced by different moment arms.

This effort was conducted using a body-fixed, six degree-of-freedom simulation (Projectile Design and Analysis Suite from Arrow Tech Associates). To characterize control authority, the flight control systems were executed in an open-loop manner. From launch, a given roll orientation (φ_P) was prescribed as the direction in which the control normal force was exerted (which dictated the direction of maneuver). Figure 2 depicts the view from the back of the projectile, illustrating a commanded control normal force in a particular roll orientation. Note that due to gyroscopic action, the projectile response is not necessarily in the direction of the control force for a spin-stabilized projectile.
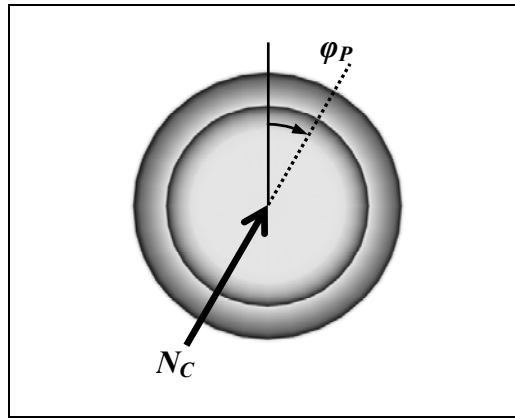

Figure 2. Control normal force directed along
prescribed roll orientation.

The continuous flight control system (denoted as C) is simply the implementation of this general model of a control mechanism for a given commanded roll orientation, with the control forces and moments in an inertial reference frame. Figure 3 shows a block diagram of the continuous flight control system. The dotted rectangular regions in the figure summarize the function of particular subgroupings of blocks. The equations for this flight control system demodulate the roll signal to appropriately calculate control forces and moments since the continuous flight control system prescribes control forces and moments in an inertial reference frame and the six degree-of-freedom equations of motion in the simulation are body fixed.

Input to this control system includes the commanded roll orientation of the control normal force and the updated roll orientation of the projectile. The roll orientation would be derived from a sensor assumed to provide a perfect signal in this study.

Output of the continuous control system includes control forces and moments in the body-fixed reference frame. These control forces and moments are summed, along with aerodynamic and
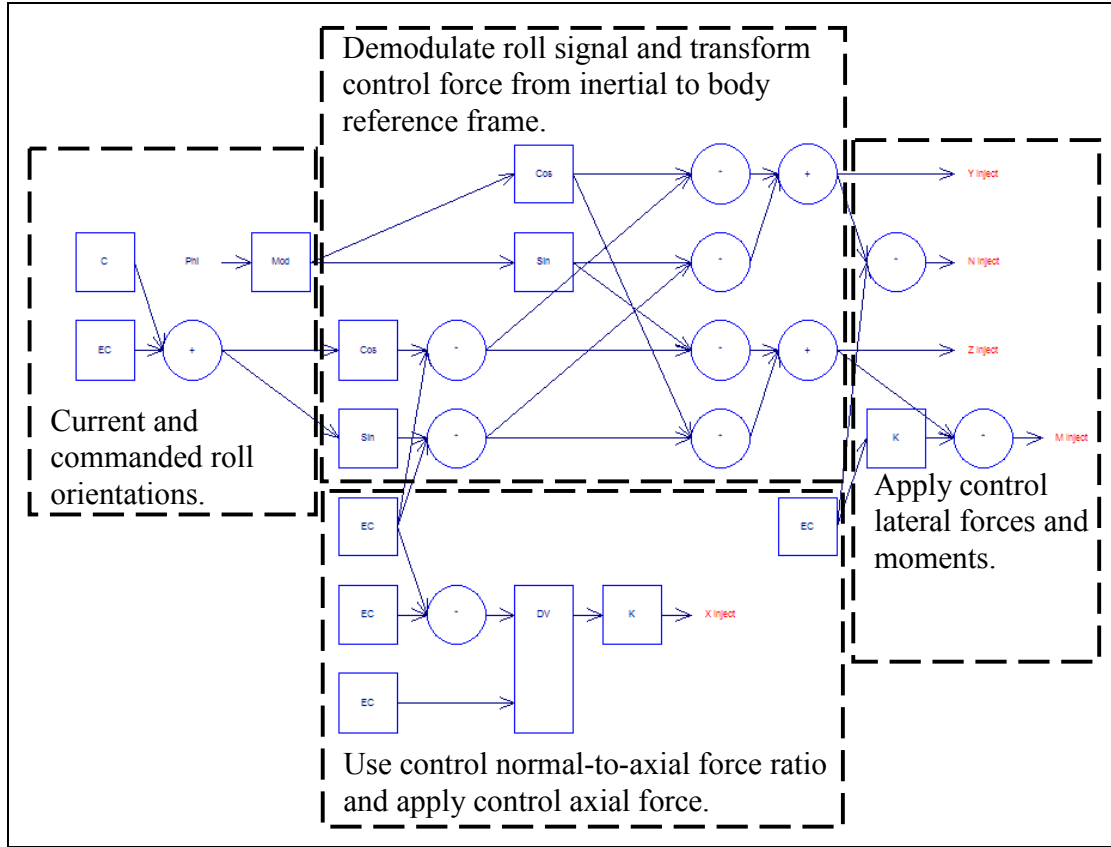
Figure 3. Flight control system block diagram for continuous case.

gravitational forces and moments in the equations of motion, to yield the motion of the flight vehicle with control.

The pulsed flight control system exerts control forces and moments only over a given window of the entire roll cycle. For example, the roll window over which the control is active (denoted as φ_C) might only be 90°. In this case, control is applied for ±45° around the commanded roll orientation. A schematic of this is presented in figure 4.

The pulsed flight control system (denoted as P) implements the control mechanism model with control forces and moments in the body-fixed reference frame and over the prescribed roll window. The block diagram of the pulsed flight control system is given in figure 5, along with some comments associated with the purpose of specific blocks. The logic of this flight control system is concerned with determining whether the roll orientation of the projectile is within the roll window before applying control forces and moments. Input and output to this flight control system are the same as the continuous case.
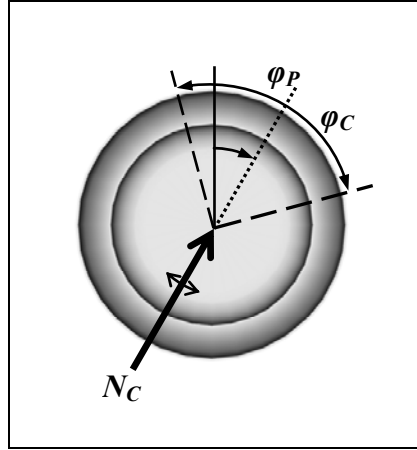
Figure 4. Roll window for pulsed
flight control system.

Current and
commanded roll
orientations and
roll window.

Apply control
forces and
moments.

Determine whether current roll orientation is
within the roll window.
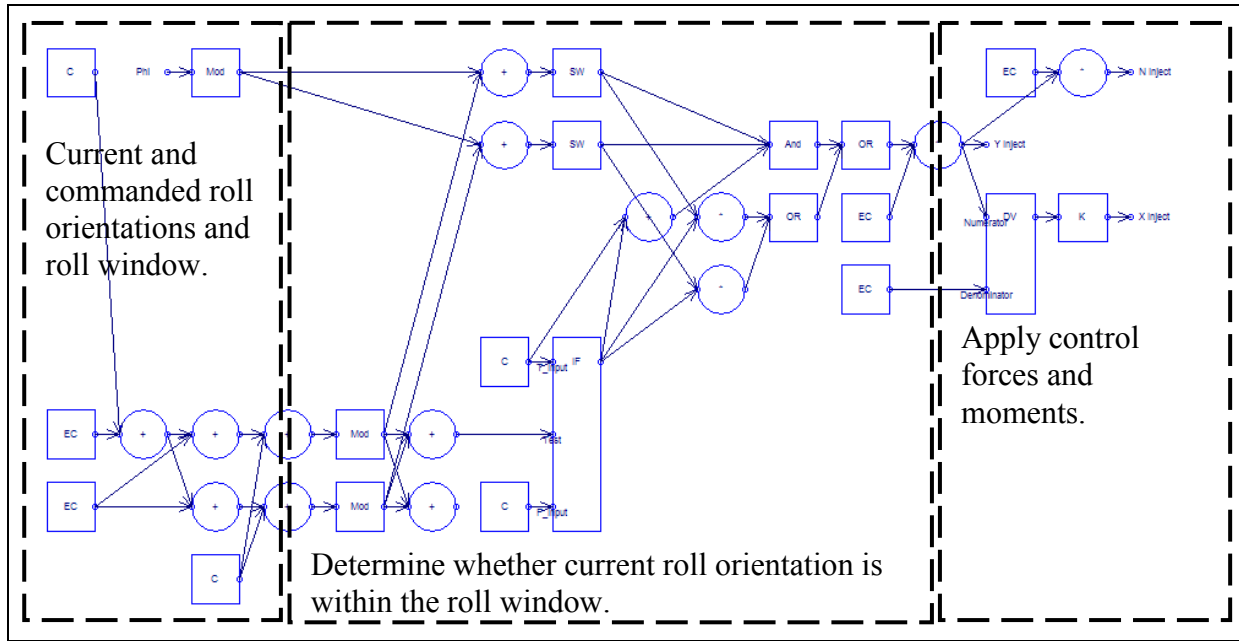
Figure 5. Flight control system block diagram for pulsed case.

To summarize the continuous and pulsed flight control systems, both systems implemented the
control mechanism model by producing forces and moments in the body-fixed reference frame.
Input consisted of commanded roll orientation, parameters (e.g., control normal force, the control
axial location on the projectile, and the control normal-to-axial force ratio), and current roll
orientation. Output was the control forces and moments.

3. Results and Discussion

The initial conditions of all simulations are provided in table 2. Launch disturbances (initial pitch, yaw, pitch rate, yaw rate, and transverse velocities) were set to zero.

Table 2. Initial conditions.

Quadrant Elevation (deg)	Muzzle Velocity (m/s)	Spin at Muzzle (Hz)
36.22	807.0	263.0

The parameters considered in this effort were the magnitude of the control normal force, the control axial location on the projectile, the control normal-to-axial force ratio ($N/A|_C$), and the roll window over which the pulsed controller operated. The control axial force (drag) was obtained by dividing the control normal force by the control normal-to-axial force ratio. The values chosen for these parameters are presented in table 3.

Table 3. Parametrics.

N_C (N)	X_C (calibers From CG)	$N/A|_C$	φ_C (deg)
20	−1.8	0.5	30
30	−1.4	1	90
40	−0.4	10	120
50	0.0	100	180
60	0.6	∞	—
—	1.6	—	—
—	2.3	—	—
—	2.6	—	—
—	3.6	—	—

Control authority was obtained by varying the commanded roll orientation from 0° to 360° in 10° increments and recording the impact location of each simulation. The results were an elliptically shaped footprint on the ground. This characterization of performance meant that any target within the maneuver footprint could be engaged.

The functional relationship between a given parameter and the control authority was obtained by assuming that the maneuver footprint was an ellipse. Major and minor ellipse axes were calculated and used to determine the area within the maneuver footprint. A sufficient number of commanded roll orientations were utilized to validate this assumption. The total AOA history was also examined to understand the connection between AOA and control authority for various parameters.

7

The baseline ballistic (no control) flight dynamics were determined. Figures 6 and 7 present the trajectory. Uncontrolled, the projectile flew over 20 km downrange and reached an altitude of about 5.5 km. Figure 7 shows that projectile drift acts to pull the munition over 500 m to the right of the line of fire.

Projectile drift resulted from the yaw of repose, a phenomenon that involves gravity, spin, and the pitching moment of the projectile. The nose of the projectile always slightly lagged the action of gravity to pull the projectile earthward, resulting in a small pitch angle. Normal force acting at the CP appeared due to this pitch angle. The CP location was forward of the CG since the projectile was statically unstable (spin stabilized). Thus, the normal force at the CP (realized as a pitching moment) tended to rotate the nose up for a positive pitch angle. The projectile acted as a gyroscope due to the high spin rate, so the net result was a moment 90° out of phase with the pitching moment. This caused the yaw of repose, nose to the right (when viewed from behind) for a positive pitch angle, which became apparent in the trajectory by the projectile drifting to the right, as seen in figure 7.
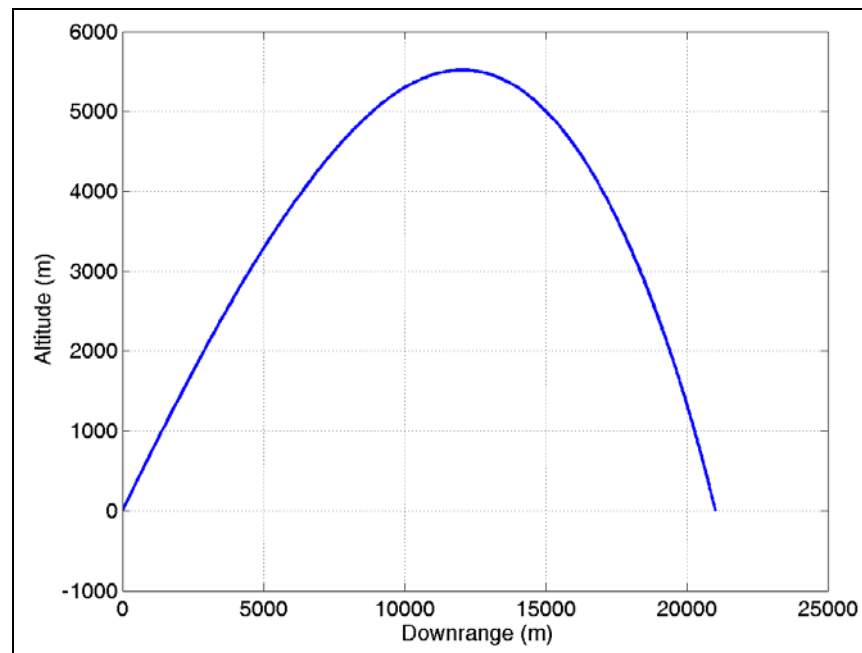

Figure 6. Vertical trajectory.

The total AOA of the ballistic flight is given in figure 8. The majority of the total AOA was in the yaw plane. Yaw of repose was maximum around apogee. A peak in total AOA of about 1.1° occurred around 30 s, which corresponded to apogee.
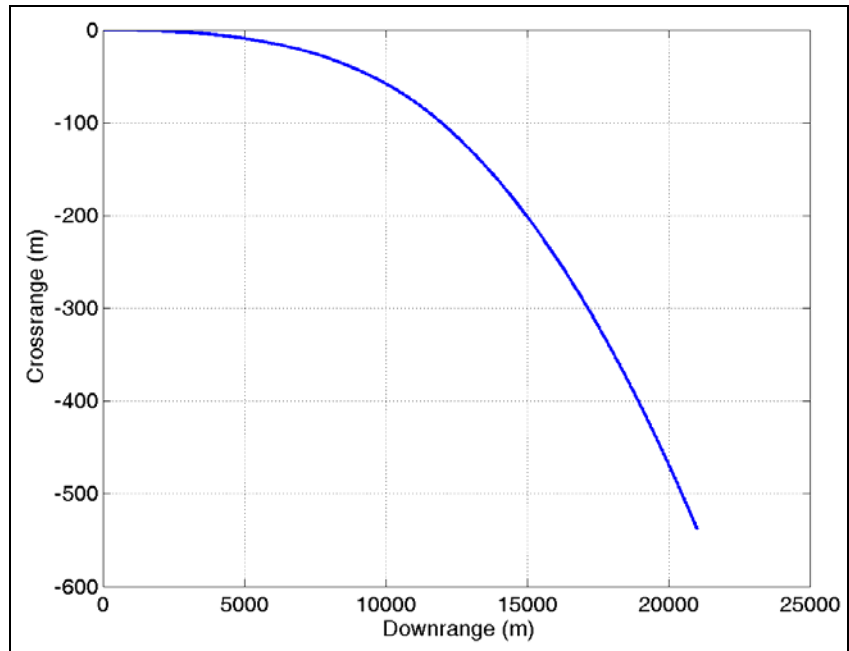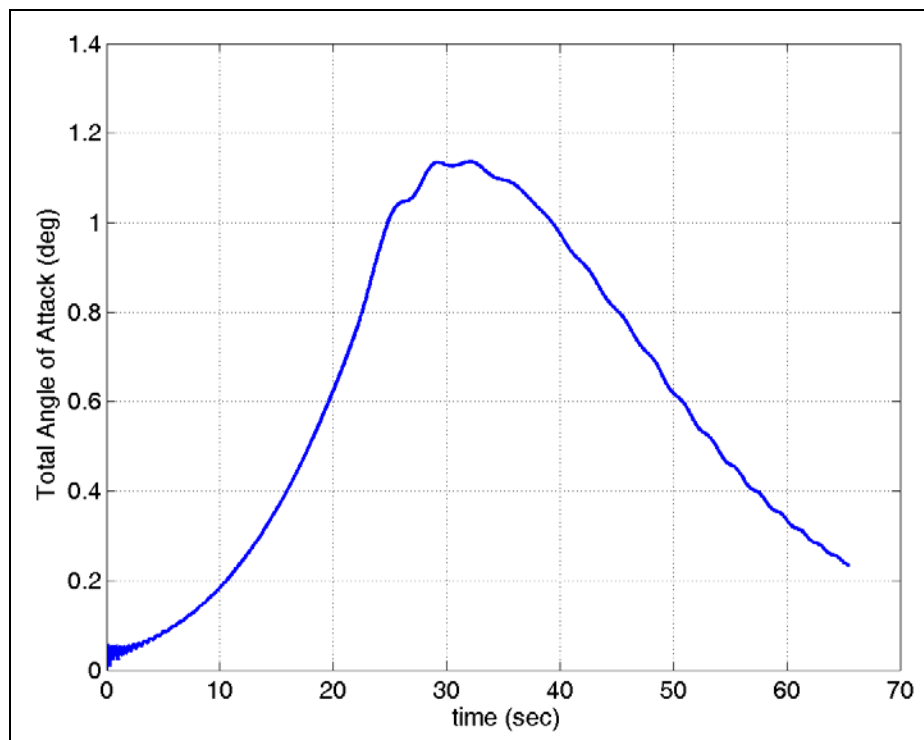
Figure 7. Horizontal trajectory.

Figure 8. Total AOA.

Controlled trajectories were obtained for prescribed values of control normal force. The control normal force magnitude was examined over a range of 20–60 N in steps of 10 N. The continuous flight control system was used, with the control location at the base of the projectile (1.8 CAL rearward of CG) and a control normal-to-axial force of infinity (corresponding to zero drag for the control mechanism).

Results for various control normal force magnitudes are provided in figure 9. The shape of the maneuver footprint for each control normal force magnitude was elliptic. The angle of fall determined whether the major and minor axes of the ellipse were oriented along the crossrange or downrange axes. The major axis of the ellipse was skewed off vertical due to yaw of repose. Essentially, when controlling the projectile up and to the right or down and to the left, the yaw of repose was added to the control-induced AOA and control authority was augmented.

As expected, figure 9 indicates that control authority increased with control normal force. The control authority scaled linearly with control normal force because the maneuver footprint boundary increased regularly by the same amount from the 20–30 N cases, the 30–40 N cases, etc.
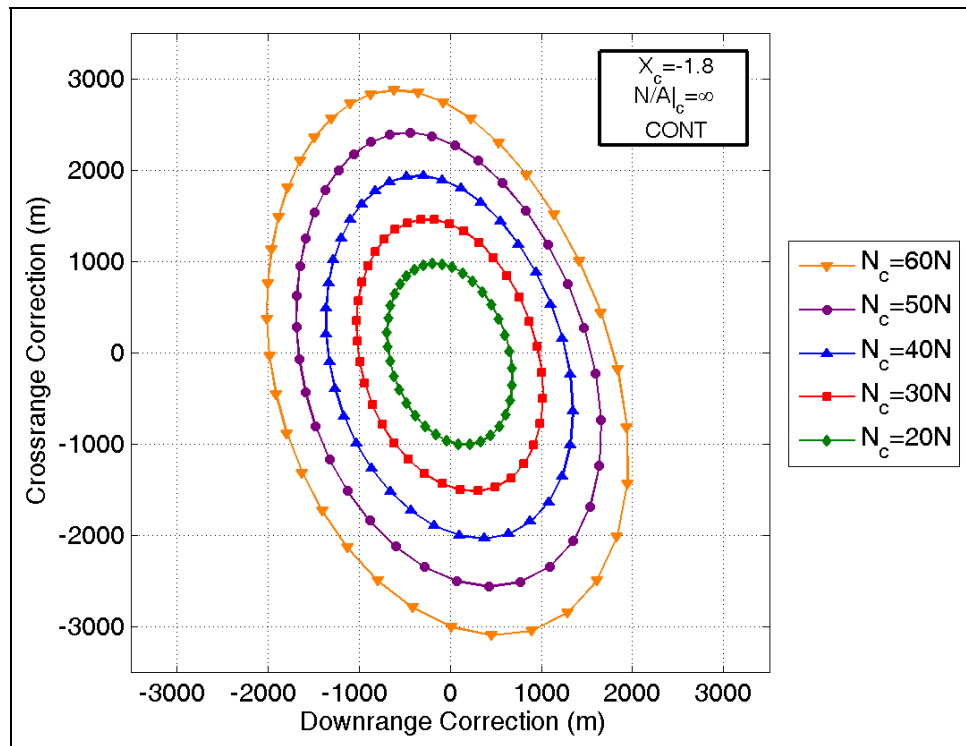

Figure 9. Maneuver footprint for control normal force parameter.

The linear relation between control authority and control normal force is confirmed by figure 10. The areas within the maneuver footprints of figure 9 were calculated and plotted as a function of control normal force. The increase in maneuver footprint area with control normal force was
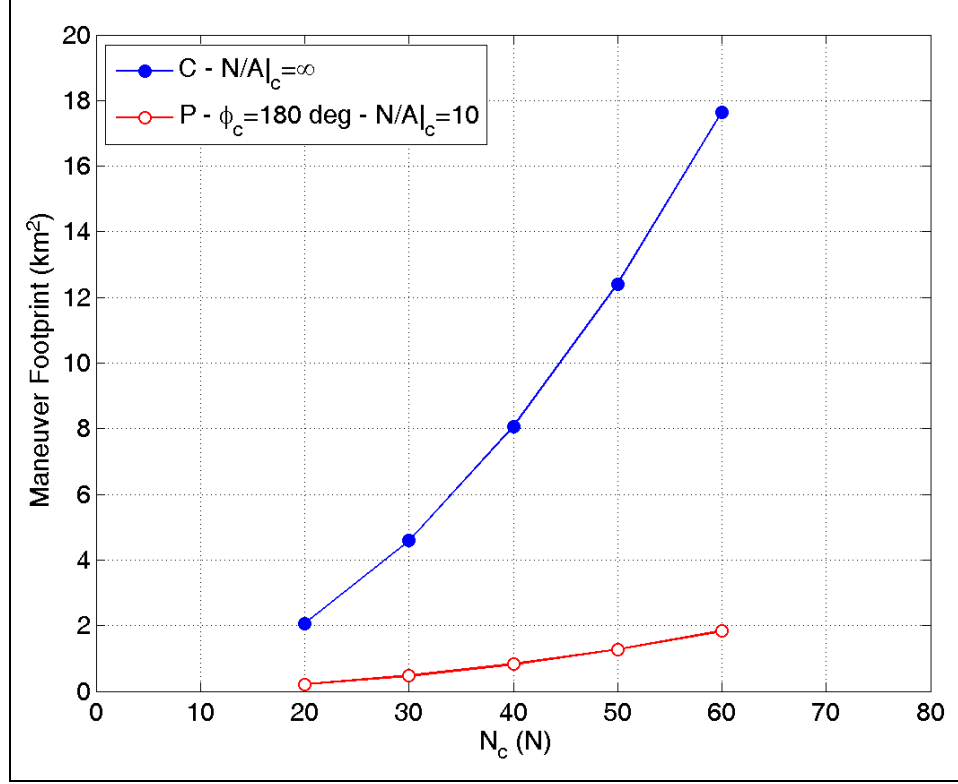
Figure 10. Relationship between maneuver footprint and control normal force.

quadratic. Therefore, control authority measured in terms of a distance was linearly related to control normal force magnitude.

Another set of calculations was performed to verify that linearity still held for the pulsed flight control system and also with the presence of a control axial force (drag). For this case, the pulsed flight control system was carried out with a roll window of 180°, control axial location at 1.8 CAL behind the CG, and a control normal-to-axial force ratio of 10. Thus, control authority distance increased linearly (and control authority area increased quadratically), with a continuous and pulsed control normal force in the absence and presence of control drag. This result was also found in closed form using linearized equations of motion by Ollerenshaw and Costello.[1]

Total AOA history for the continuous flight control system for various control normal force magnitudes is shown in figure 11. In these results, the flight control system commanded a maneuver at the 0° roll orientation throughout the flight to extend the range (i.e., control normal force pushed "up").

The overall trend of the data in figure 11 illustrates the yaw of repose as shown for the baseline ballistic flight. However, the magnitude was greater than the ballistic flight due to a control-induced AOA. When a control normal force was exerted at any location other than the CG, the projectile responded with an aerodynamic normal force at the CP. The projectile AOA
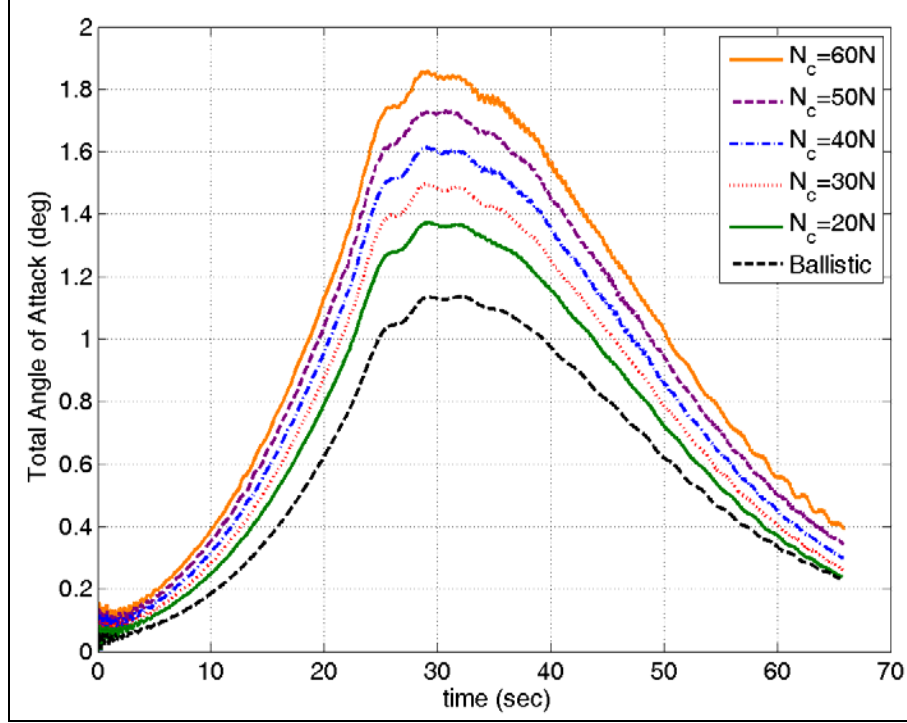
Figure 11. Total AOA history and variation with control normal force.

magnitude increased, thereby increasing the aerodynamic normal force, until the aerodynamic pitching moment (product of aerodynamic normal force and location of the CP with respect to the CG) balanced the control moment. This control-induced AOA appeared in these results as a different total AOA for the controlled cases than the ballistic case. This situation existed in the steady state and even applied to the transient results described herein.

For a control axial location at the base of a spin-stabilized projectile, increasing control force magnitude produced a larger aerodynamic moment to match a larger control moment and, ultimately, linearly increase the total AOA. This applied only in the absence of a control axial force (drag). When drag was present, a smaller control normal force could produce a larger control-induced AOA due to the influence of dynamic pressure. This will be discussed further when considering the control lift-to-drag ratio.

The control axial location was varied in the continuous flight control system, with a control normal force of 50 N and control normal-to-axial force of infinity (corresponding to zero drag for the control mechanism). It is important to note that the CP at launch (M ≈ 2.4) was near $X_C = 2.3$ and varied throughout the flight as the Mach number changed. Maneuver footprints for the control axial location parameter are presented in figure 12. The largest footprint occurred when the control was located at the base of a spin-stabilized projectile. As the control axial location moved forward, the footprint decreased to a minimum around $X_C = 2.3$ (near the CP) before increasing again with a differently shaped ellipse.
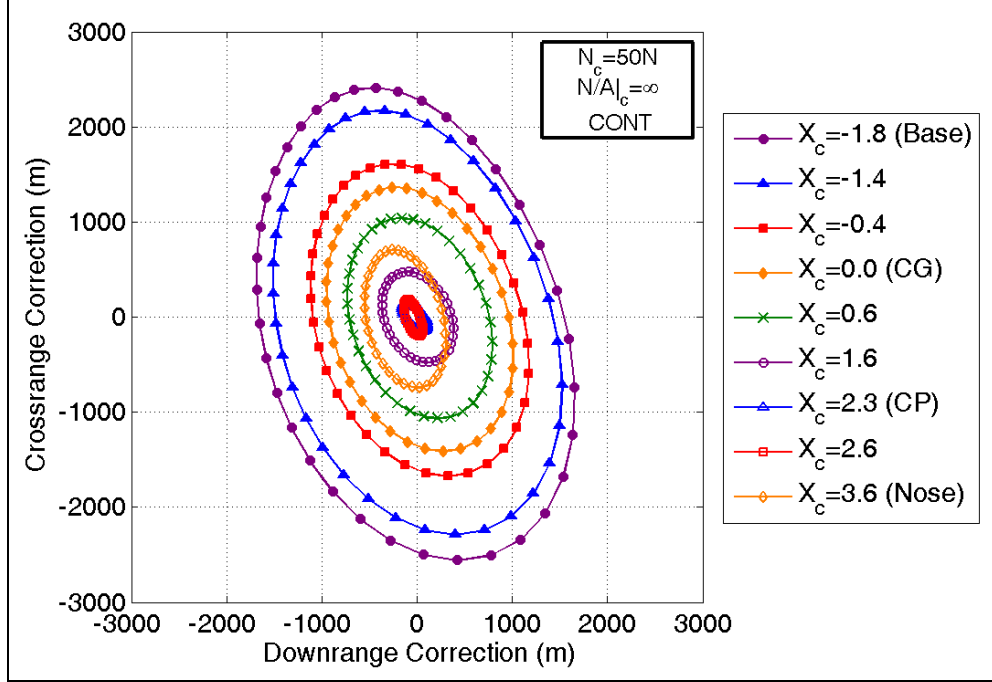
Figure 12. Maneuver footprint for the control axial location parameter.

Before describing the physics of this behavior, the relationship between maneuver footprint and control axial location is given in figure 13. This trend validates the discussion of control authority for the control axial location parameter. The footprint decreased from a maximum at the base to a minimum at the CP and increased again to a relatively lower magnitude at the nose. The relationship in the figure appeared nonlinear for this realistic situation in which the CP varied throughout the flight.

The physics involved with understanding the response of the projectile to various control axial locations relied on the earlier discussion of the control and aerodynamic forces and moments. In steady state, the control and aerodynamic moments must balance (i.e., applying a control moment will result in a balancing aerodynamic moment). Balancing control and aerodynamic moments created a relationship between control and aerodynamic forces (depicted in figure 14). In this figure, N_A is the aerodynamic force, M_A is the aerodynamic moment, and X_A is the location of the CP with respect to the CG. As previously discussed, the control forces and moments could be from aerodynamic phenomena. However, in this study, the aerodynamic forces and moments were distinguished due to all aerodynamic surfaces except for the control mechanism.

For the steady-state case, an equation can be written since the moments are simply the product of forces and moment arms.

$$N_C X_C = -N_A X_A. \tag{1}$$

13

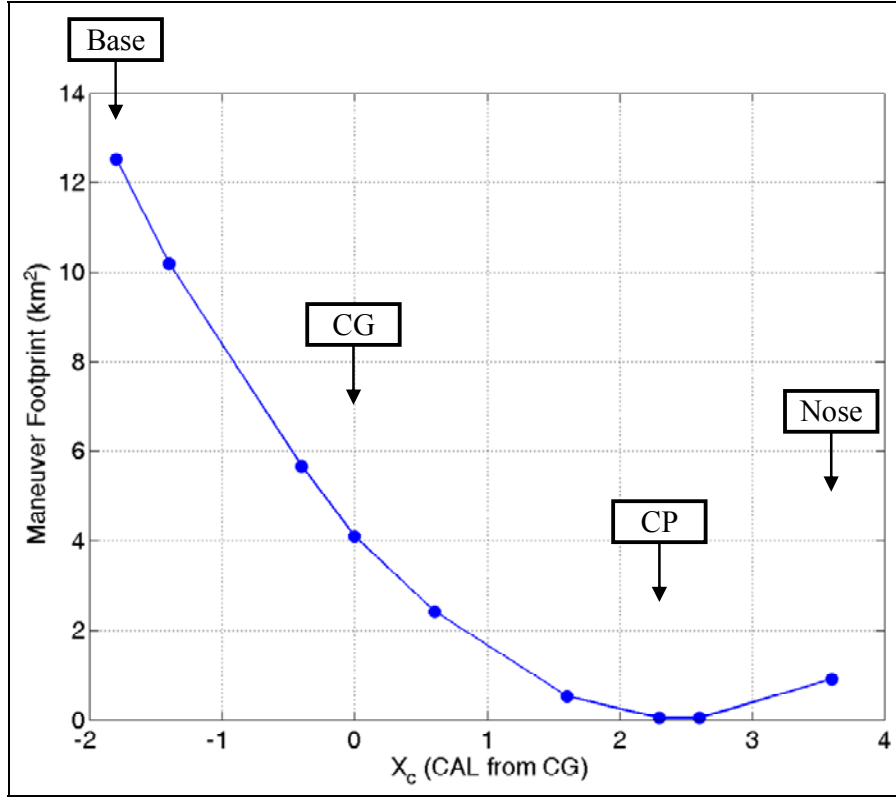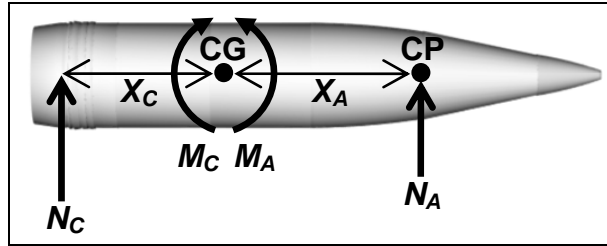Figure 13. Relationship between maneuver footprint and control axial location.

Figure 14. Illustration of control and aerodynamic
forces and moments.

This equation can be recast to solve for the aerodynamic normal force required to balance a
given control normal force at some axial location.

$$N_A = -N_C \frac{X_C}{X_A}.$$
(2)

The aerodynamic normal force obeys the following relation:

$$N_A = qSC_{N_\alpha}\alpha,$$
(3)

14

where q is the dynamic pressure, S is the reference area, C_{N_α} is the normal force coefficient, and α is the AOA. The two previous equations may be combined to estimate the control-induced AOA (α_C).

$$\alpha_C = \frac{-X_C N_C}{X_A qSC_{N_\alpha}}. \tag{4}$$

Now, the lateral motion of the controlled projectile goes as the sum of the control and aerodynamic normal forces. The total normal force (N_T) can be written as follows:

$$N_T = N_C + N_A = N_C - \frac{X_C}{X_A}N_C = \left(1 - \frac{X_C}{X_A}\right)N_C. \tag{5}$$

These two previous equations allowed the direction of the maneuver and subsequent control-induced AOA as a function of the control axial location to be understood.

Investigation of the effect of control axial location on the direction of the maneuver and control-induced AOA was considered in five cases. Each case corresponded to the control force being exerted on a different region of the projectile spin axis. For all cases, the following conditions were assumed: $N_C > 0$, $q > 0$, $S > 0$, $C_{N\alpha} > 0$, and $X_A > 0$. The last condition ($X_A > 0$) held for spin-stabilized projectiles, and the opposite ($X_A < 0$) was true for a fin-stabilized projectile. Table 4 presents the magnitude of the total normal force, direction of the maneuver, and direction of the control-induced AOA.

Table 4. Maneuver direction and control-induced AOA for various control axial locations.

Case	X_C	N_T	Maneuver Direction	α_C
Control behind CG	$X_C < 0$	$N_C < N_T$	Positive, same as N_C	$0 < \alpha_C$
Control at CG	$X_C = 0$	$N_C = N_T$	Positive, same as N_C	$\alpha_C = 0$
Control between CG and CP	$0 < X_C < X_A$	$0 < N_T < N_C$	Positive, same as N_C	$\alpha_C < 0$
Control at CP	$X_C = X_A$	$N_T = 0$	No maneuver	$\alpha_C < 0$
Control forward of CP	$X_A < X_C$	$N_T < 0$	Negative, opposite N_C	$\alpha_C < 0$

When the control axial location was behind, the CG of the control-induced AOA was positive so that the total normal force was the sum of the control normal force and aerodynamic normal force. Maneuver direction was in the same direction as the control force. No control-induced AOA was generated when control normal force was at the CG because there was no control

moment. As a result, the total normal force was simply the control normal force, and lateral motion was in the same direction as the control force.

For control force between the CG and CP, the control-induced AOA was negative since the control force was forward of the CG. Control and aerodynamic normal forces acted in opposite directions. The maneuver direction was still in the same direction as the control force since the oppositely directed aerodynamic normal force had a lower magnitude than the control force.

When the control was oriented precisely at the CP, the control-induced AOA was still negative. However, the control and aerodynamic forces precisely cancelled to produce no lateral motion. As the control force moved ahead of the CP, control-induced AOA was negative and the aerodynamic normal force increased above the control force. The direction of the maneuver was now opposite the direction of the control force.

This discussion explained the behavior seen in figures 12 and 13. The largest control authority was with control at the base of the projectile. Here, control and aerodynamic normal forces acted in the same direction. Since X_C was the largest negative number, then the control-induced AOA and aerodynamic normal force were maximums. Since the total normal force decreased, control authority decreased as the control location moved forward of the base. For control locations near the CP, control authority was a minimum since the control and aerodynamic normal forces were offset. As the control location moved forward of the CP, the control authority increased with a differently shaped footprint. The change in footprint shape for X_C forward of the CP occurred because flight vehicle response with commanded roll orientation was reversed (e.g., a control command "up" resulted in a maneuver "down"). This behavior was described by Ollerenshaw and Costello.[1]

The influence of the control normal-to-axial force ratio (or, alternatively, the lift-to-drag ratio of the control mechanism) was examined. The continuous flight control system was exercised for a control normal force of 50 N and a control axial location of 1.8 CAL rearward of the CG. By varying the normal-to-axial force ratio with a constant normal force, the effect of axial force (drag) of the control mechanism was able to be inferred. Recall that the control forces were applied along the spin axis and, therefore, control axial force did not contribute to the control moment.

Higher drag control mechanisms (lower control normal-to-axial force ratio) might have a larger maneuver footprint when the control forces were applied later in the flight (recall that control was applied from launch in this study). The relative influences of the control normal force to increase range and the control axial force to decrease range determined this behavior. Calculation of optimal control application along the trajectory for a given control normal-to-axial force ratio was not investigated.

The lift-to-drag ratios of some control mechanisms are available in the literature. Blades, such as canards, fins, and wings, have an order of magnitude of lift-to-drag ratio of around 10. High-

drag devices, such as tabs extending out of the body normal to the flow direction, might be more on the order of 1 or less for a lift-to-drag ratio. Alternatively, thrusters might feature a lift-to-drag ratio higher than 10. The range of control normal-to-axial force ratios used in this report were constructed to span this practical range and also investigate the limit of a zero-drag control mechanism ($N/A|_C = \infty$).

Maneuver footprints for varying control normal-to-axial force ratios are provided in figure 15. When drag of the control mechanism was negligible ($N/A|_C = \infty$), the footprint was largest and centered on the origin. As drag increased (decreased $N/A|_C$), the footprint decreased and shifted to the left. The leftward shift amounted to a reduction in the range of the projectile when the drag of the control mechanism was considered. This result indicated that a high-drag control mechanism might provide satisfactory control authority at the expense of a reduced range.
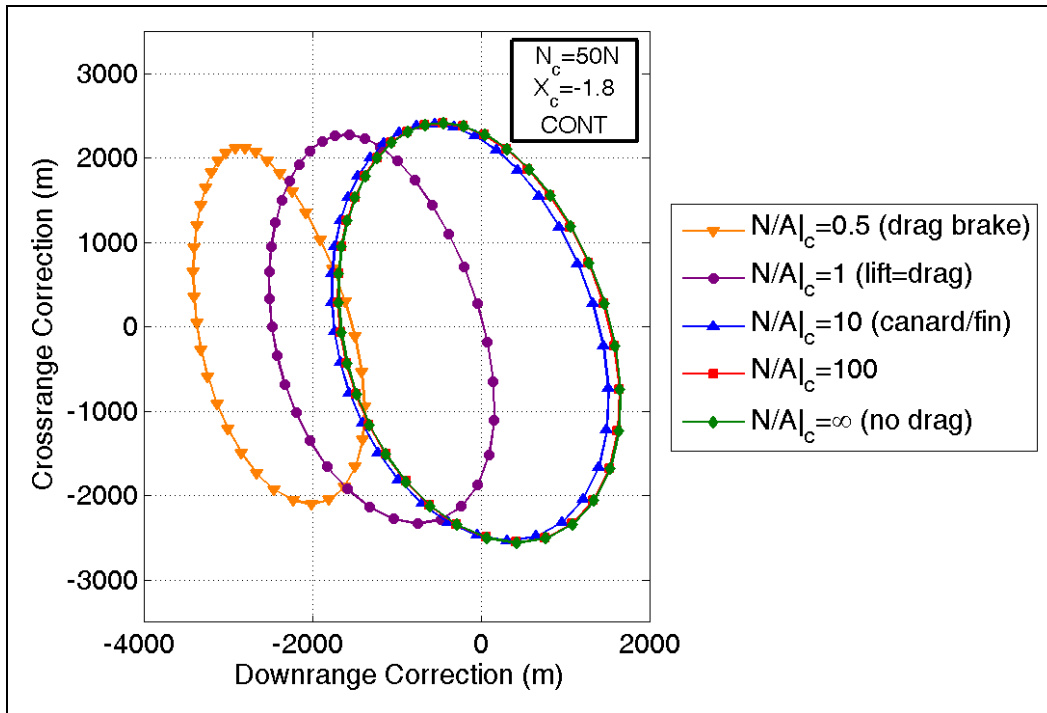

Figure 15. Maneuver footprint for the control normal-to-axial force ratio parameter.

Figure 16 presents the relationship between maneuver footprint and a control normal-to-axial force ratio. For high lift-to-drag control mechanisms ($N/A|_C = 10$, 100, and 10^8), the maneuver footprint was a little over 12 km^2. The footprint featured an asymptote as the control normal-to-axial force ratio went to infinity. For $N/A|_C \geq 10$, the axial force was much lower than the normal force of the control mechanism and negligibly contributed to the overall motion. Thus, optimizing the lift-to-drag ratio of the control mechanism significantly above 10 might not appreciably increase control authority.
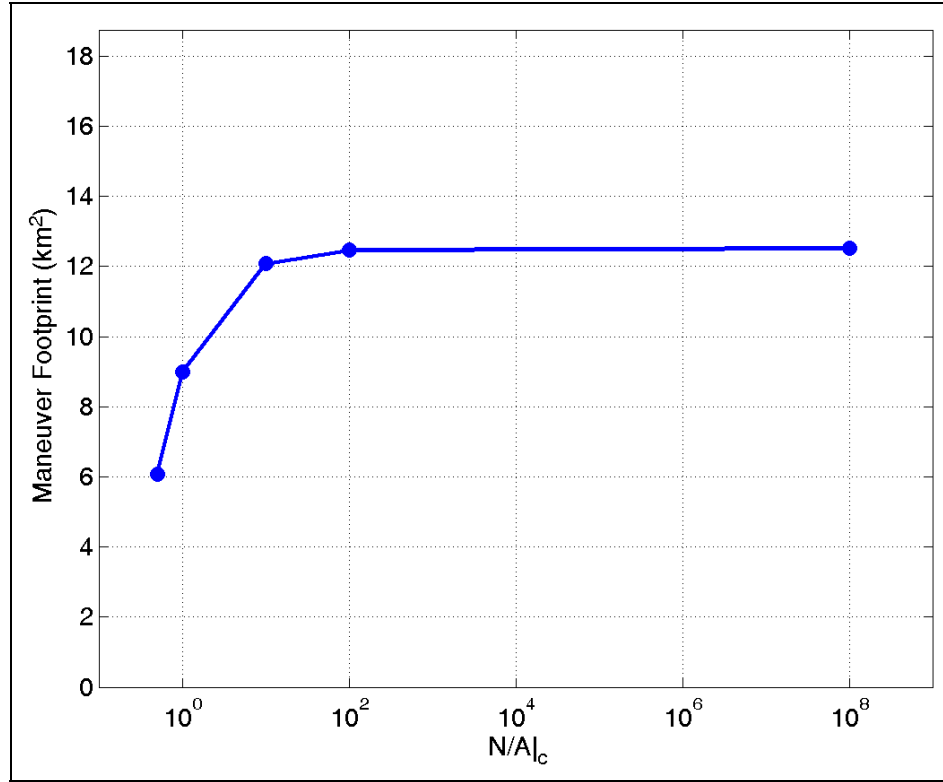
Figure 16. Relationship between maneuver footprint and the control normal-to-axial
force ratio.

As the control normal-to-axial force ratio decreased, however, the control authority nonlinearly decreased and sharply reduced for ratios less than unity. When the control normal-to-axial force ratio was an order of one or less, the axial force became significant. Investments in design changes to slightly increase the control normal-to-axial force ratio might pay off in considerably increased control authority.

As the lift-to-drag ratio of the control mechanism decreased, the maneuver footprint and the average range of the footprint also decreased. To quantify this effect, the center of each maneuver footprint given for the control normal-to-axial force ratio parameter was calculated and subtracted from the range of the baseline ballistic flight. The result was tabbed as the range decrease.

These range reductions are given as a function of the control normal-to-axial force ratio in figure 17. The trend in this data matched that shown for maneuver footprints. High lift-to-drag ratio control mechanisms ($N/A|_C \geq 10$) did not appreciably decrease range. A nonlinear decrease in range with control normal-to-axial force ratio occurred for $N/A|_C \leq 1$. Here, a relatively higher control axial force decreased the velocity of the projectile. Lower velocity translated directly into decreased range. These results showed that a sufficient control authority might be obtained with a low lift-to-drag control mechanism; however, the maximum range might be drastically reduced.
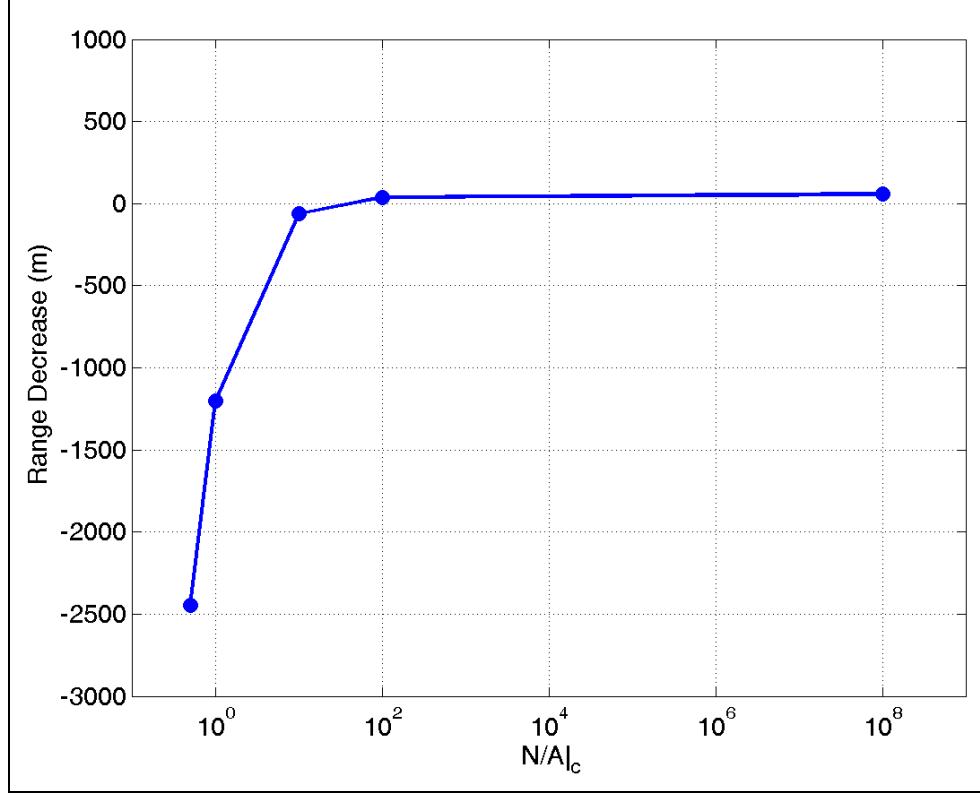
18

Figure 17. Relationship between range decrease and the control normal-to-axial force ratio.

The total AOA behavior with varying control normal-to-axial force ratios is provided in figure 18. These data showed similar total AOA history for $N/A|_C \geq 10$. Total AOA increased as the control normal-to-axial force ratio decreased for $N/A|_C \leq 1$.

The explanation of these dynamics was related to the control axial force and the balance of control and aerodynamic moments. Because control axial force increased, projectile velocity decreased, with a decreased normal-to-axial force ratio. (Note that dynamic pressure goes as a quadratic with the velocity [$q = 1/2 \rho V^2$].) The control normal force and control axial location remained the same between cases. Therefore, an equal control moment existed for the aerodynamic moment to balance. The aerodynamic normal force must stay the same since the CP and CG separation (moment arm of the aerodynamic moment) was also the same for all cases. According to the standard relation for aerodynamic normal force ($N_A = qSC_{N\alpha}\alpha$), the AOA must increase for an equal normal force with lower dynamic pressure and equal reference area and coefficient of normal force. As the control normal-to-axial force ratio decreased in figure 18, the nonlinear increased in total AOA.

A comparison of the continuous and pulsed flight control systems, along with an exploration of the effect of the roll window on the pulsed system, was undertaken. These cases featured a control normal force of 50 N, control axial location at the rear of the projectile (−1.8 CAL from CG), and a control normal-to-axial force ratio of infinity.
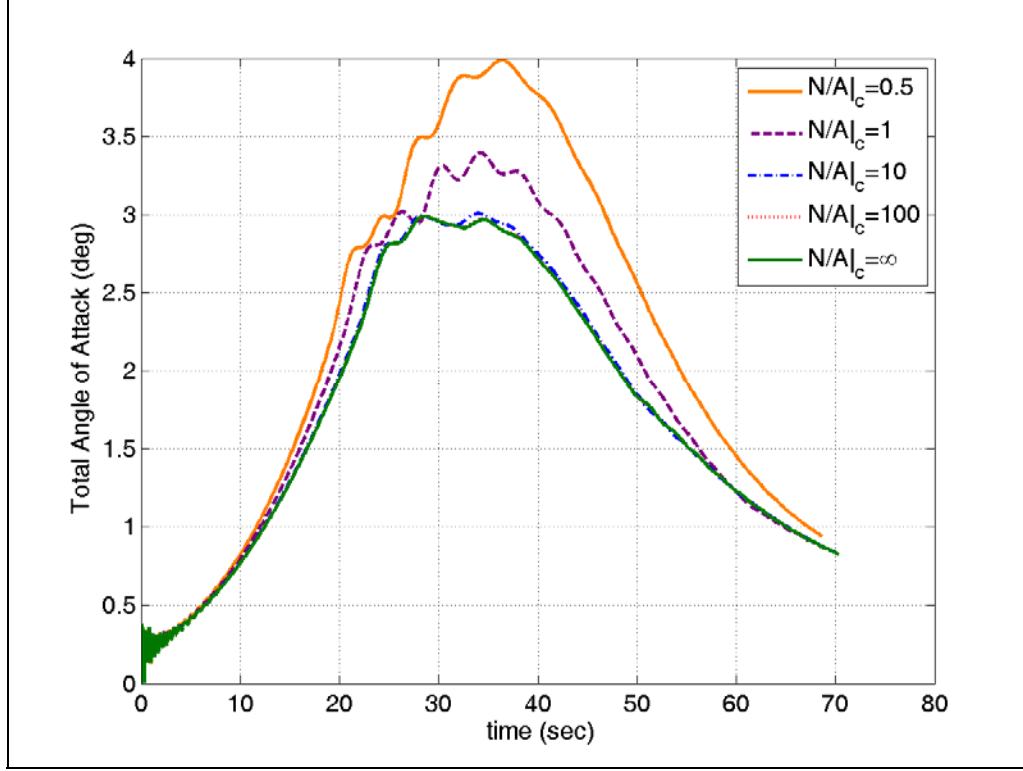
Figure 18. Total AOA history and variation with the control normal-to-axial force ratio.

The results shown in figure 19 highlight the marked increase in the maneuver footprint for the continuous flight control system over the pulsed system. Despinning the control mechanism to ensure that the control normal force was oriented in the same inertial orientation throughout the flight yielded a large return in control authority. In contrast, the pulsed flight control system with a 30° roll window was the smallest footprint. Increasing the roll window from 30° to 90° resulted in an appreciable increase in control authority. However, increasing the roll window further to 120° and 180° only slightly increased the footprint.

These variations in maneuver footprint with continuous and pulsed flight control systems are quantified in figure 20. Because of the large difference in magnitude of the maneuver footprint between the continuous and pulsed flight control system, only the pulsed control system results were shown. The continuous flight control system had a footprint of about 12.5 km^2. The pulsed case with the largest footprint ($\varphi_C = 180°$) had an order of magnitude lower footprint than the continuous flight control system. As roll window decreased from 180° to 120°, 90°, and 30°, the control authority decreased.

The variation in control authority with roll window for the pulsed flight control system was due to the amount of roll cycle over which the control forces and moments were active and the control-induced AOA when the control was active.
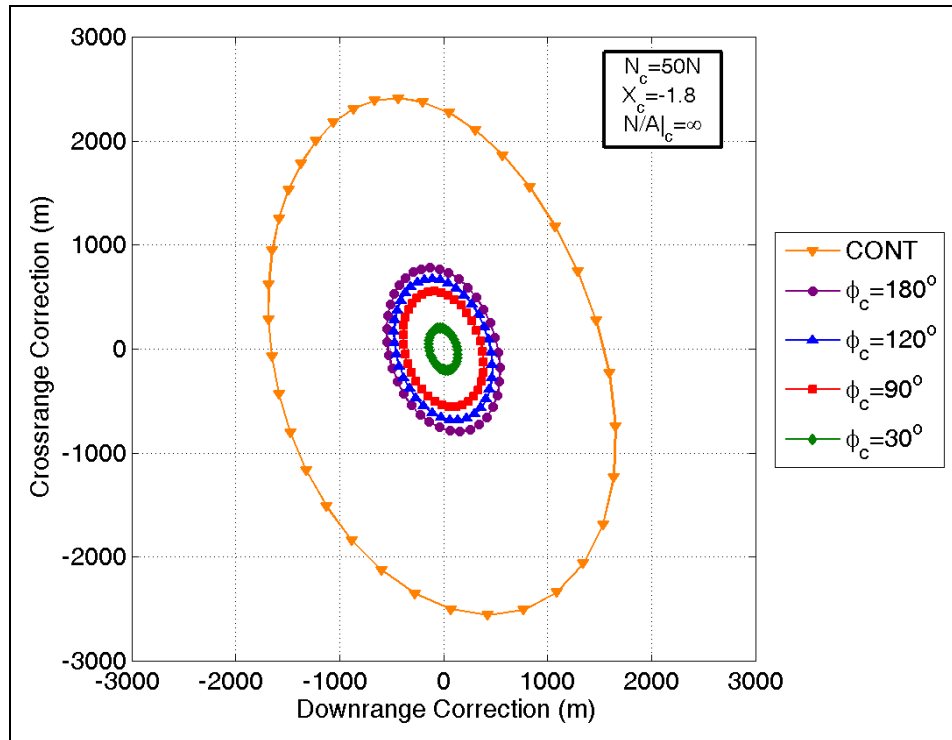
Figure 19. Maneuver footprint for continuous and pulsed flight control systems with the roll window parameter.
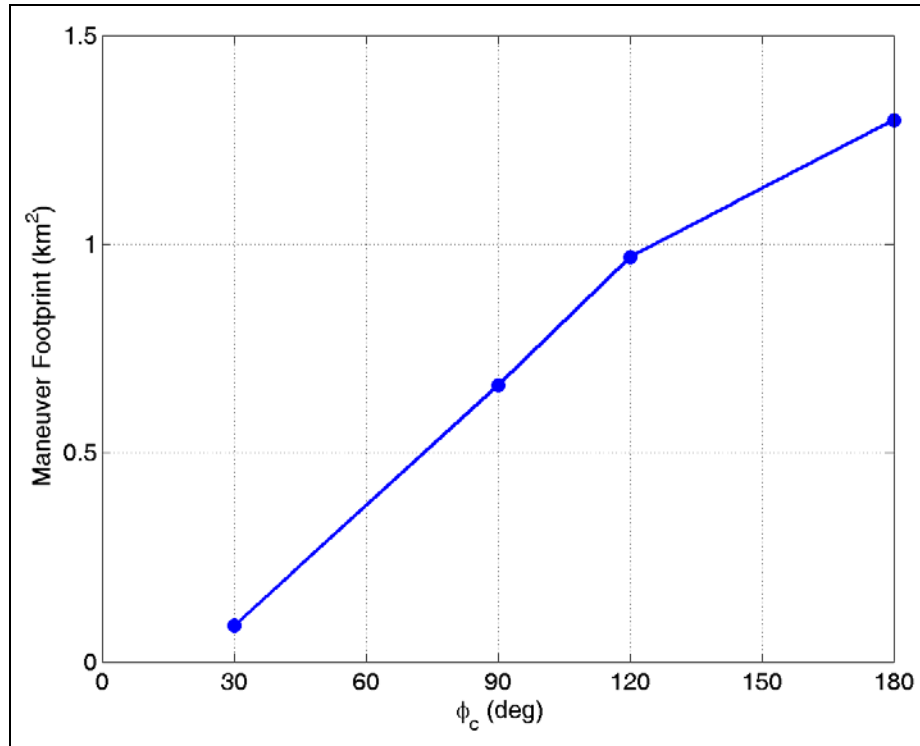

Figure 20. Relationship between maneuver footprint and continuous and pulsed flight control systems with the roll window parameter.

21

The first effect can be understood by deriving a simple mathematical relation for the scale of pulsed normal force exerted over a roll cycle. The average dimensionless pulse strength (P^*), or magnitude of the normal control force averaged over a complete roll cycle, can be written as the integral of the normal force signal ($f(\varphi)$) over the duration of operation (φ_C) and normalized by one cycle (2π).

$$P^* = \frac{1}{2\pi} \int_{\varphi - \varphi_C/2}^{\varphi + \varphi_C/2} f(\varphi) d\varphi . \tag{6}$$

For the continuous flight control system, $\varphi_C = 180°$ and $f(\varphi) = 1$ since the control normal force was active for the entire flight and oriented in the same inertial direction. When this function was placed in the previously mentioned relation, $P^* = 1$ for the continuous flight control system. For the pulsed flight control system, $f(\varphi) = \sin\varphi$ since the body-fixed control normal force direction rolled with the body.

Thus, the mathematical expression for P^* enabled a determination of the behavior of control authority by isolating the influence of pulse duration. Various roll windows were integrated in the previous equation, and the results were plotted in figure 21. These results showed that the 30° pulse controller was about 9% as effective as the continuous flight control system. The effectiveness increased nonlinearly with roll window and eventually reached an asymptote of about $P^* = 0.31$ for $\varphi_C = 180°$. The trend in the curve of figure 21 matched the one in figure 20.

The pulse controller was less effective as the roll window increased for higher values of φ_C (>90°) because of the orientation of the body-fixed control normal force. As $\varphi_C \rightarrow 180°$, more of the control normal force was oriented normal to the commanded roll orientation and resulted in less lateral motion. Note that control authority could be increased by placing several control mechanisms at different radial locations to effectively increase the pulse duration.

Decreased pulse duration also decreased control authority by reducing the control-induced AOA. Figure 22 shows that the total AOA increased as the roll window increased. Control authority decreased for the pulsed flight control system due to lower control duration per cycle and lower total AOA when active.

4. Conclusions and Implications

The development of gun-launched smart munitions features many unique challenges. The dynamics of spin-stabilized precision munitions are fundamentally different than more conventional fin-stabilized smart weapons and must be properly accounted for to achieve a successful design. This effort helps the designers of smart munitions by exploring the physics of control mechanism strategies for spin-stabilized projectiles.
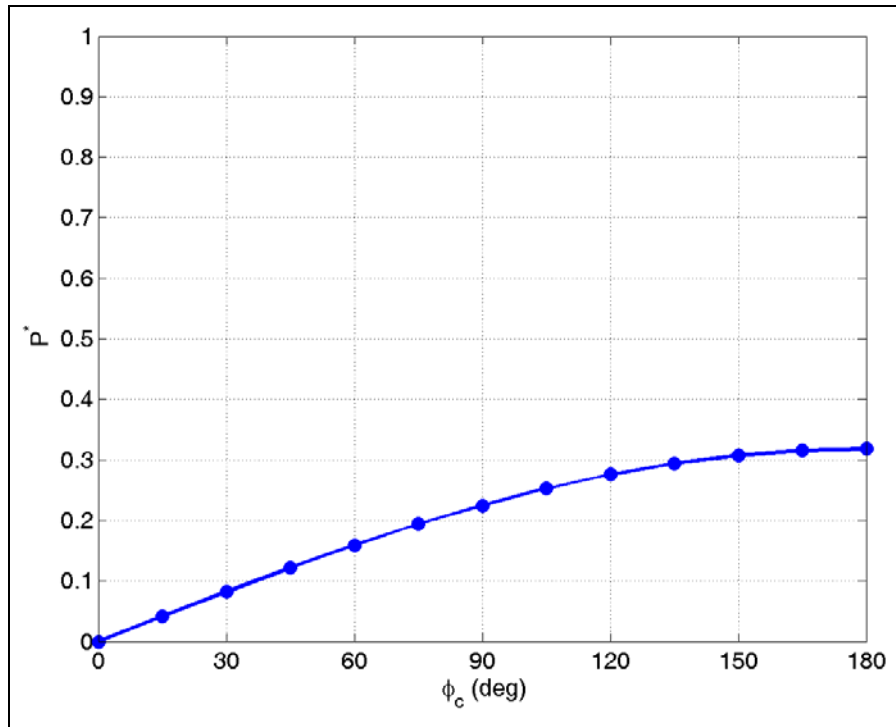
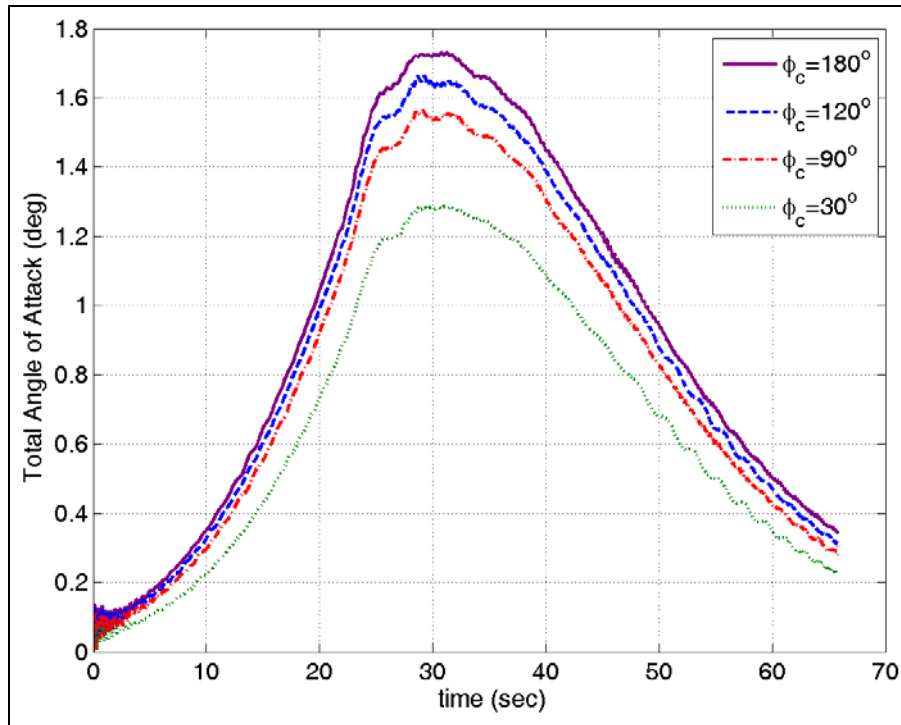Figure 21. Relationship between the average dimensionless pulse strength and roll window parameter.

Figure 22. Total AOA history and variation with the pulsed flight control system roll window parameter.

A typical 155-mm artillery round and the associated flight dynamics were selected as the test bed to understand the effects of control normal force magnitude, control axial location, control normal-to-axial force ratio, and roll window for a pulsed and continuous flight control system. Control authority was characterized by open-loop maneuvers in a six degree-of-freedom environment.

Simulation results were supported by mathematical modeling of the physical processes such as the generalized dynamics of spin-stabilized projectiles, with variations in control mechanisms (e.g., control force, moment, lift-to-drag ratio, and roll window). Discussions of the basic physics also included yaw of repose and projectile drift.

The maneuver footprint shape was dictated by the angle-of-fall and yaw of repose. Shallow angles-of-fall produced footprint ellipses, with a major axis oriented along the downrange axis and vice versa. Bulges in the footprint "up and to the right" and "down and to the left" were caused by an augmentation in control authority due to yaw of repose.

Control authority increased linearly with control normal force. Thus, by increasing the normal force of the control mechanism by some amount (e.g., by increasing the platform area of a control surface or momentum flux of a thruster), the associated maneuver could be expected to increase by a linearly related amount.

Control authority varied nonlinearly, with a wide variation in magnitude, and with control axial location. Control from the base produced the largest maneuver footprint. Locating control at the CG did not produce any control-induced AOA. Controlling at the CP minimized control authority. Placing the control mechanism forward of the CP generated a net motion in the opposite direction from the control normal force. All of these truths were artifacts of the interaction of the control and aerodynamic normal forces and associated control-induced AOA. The relative magnitude of the maneuver footprints indicated the consequences of suboptimal control location due to overarching weapon system trade-offs.

It should be noted that in practical applications, the net control force axial location was usually not at the location of the control mechanism due to aerodynamic interference effects. As an example, exploding a pyrotechnic device (e.g., squib) produced an impulsive force at the mounting location. However, the ejecta also distorted the boundary layer locally and affected the flow downstream over surfaces such as fins. The net effect was a control force, moment arm, and moment different than that solely due to the squib chemical energy and mounting location. For this reason, the control axial locations in this study were the resultant force locations and not necessarily the location of the actual physical control mechanism.

Recall that the control normal-to-axial force ratio was akin to a lift-to-drag ratio, which could be found for various classes of control mechanisms in the literature or obtained for specific configurations via a wind tunnel, computational fluid dynamics, or free-flight testing. Control authority varied nonlinearly with the control normal-to-axial force ratio. Maneuver footprint and

range decrease were insensitive to control normal-to-axial force ratios of 10 or more. Time spent increasing the control mechanism lift-to-drag ratio did not benefit control authority for ratios of about 10 or more.

Increased drag strongly decreased control authority and range for control normal-to-axial force ratios of about 1 or less. Thus, slight increases in lift-to-drag ratio resulted in appreciable increases in effectiveness. Sufficient control authority may be achieved with a low lift-to-drag ratio control mechanism if reduced range is tolerable. The control-induced AOA also increased nonlinearly with the decreasing control normal-to-axial force ratio.

The continuous flight control system featured a fundamental advantage in control authority over the pulsed case because the control normal force was always oriented in the same inertial direction. Conversely, for the pulsed case, the control normal force was exerted for only a portion of the roll cycle; this force rotated with the body when active.

The advantages of a continuous over a pulsed flight control system were quantified. The complexity added by despinning the control mechanism may be warranted if significant control authority (or range extension) is crucial to weapon system performance. For the pulsed flight control system, the maneuver footprint varied nonlinearly with roll window due to the pulse time and control-induced AOA. Furthermore, the increasing roll window became less effective as the roll window reached 180° due to the misalignment in the directions of the body-fixed normal control force and the commanded roll orientation.

NO. OF
COPIES   ORGANIZATION

1   DEFENSE TECHNICAL
(PDF   INFORMATION CTR
only)   DTIC OCA
        8725 JOHN J KINGMAN RD
        STE 0944
        FORT BELVOIR VA 22060-6218

1   US ARMY RSRCH DEV &
        ENGRG CMD
        SYSTEMS OF SYSTEMS
        INTEGRATION
        AMSRD SS T
        6000 6TH ST STE 100
        FORT BELVOIR VA 22060-5608

1   DIRECTOR
        US ARMY RESEARCH LAB
        IMNE ALC IMS
        2800 POWDER MILL RD
        ADELPHI MD 20783-1197

1   DIRECTOR
        US ARMY RESEARCH LAB
        AMSRD ARL CI OK TL
        2800 POWDER MILL RD
        ADELPHI MD 20783-1197

1   DIRECTOR
        US ARMY RESEARCH LAB
        AMSRD ARL CI OK T
        2800 POWDER MILL RD
        ADELPHI MD 20783-1197

ABERDEEN PROVING GROUND

1   DIR USARL
        AMSRD ARL CI OK TP (BLDG 4600)